






Quest for understanding neutron emission in nuclear fission: The case of ^{210}Po Sangeeta Dhuri ^{1,2}, K. Mahata ^{1,2,*}, K. Ramachandran,¹ P. C. Rout,^{1,2} A. Shrivastava ^{1,2}, S. K. Pandit,^{1,2} V. V. Parkar,^{1,2} Shilpi Gupta ^{1,2}, V. V. Desai ^{1,†}, A. Kumar,¹ E. T. Mirgule,^{1,‡} B. K. Nayak,^{1,2} and A. Saxena¹¹*Nuclear Physics Division, Bhabha Atomic Research Centre, Mumbai - 400085, India*²*Homi Bhabha National Institute, Anushaktinagar, Mumbai - 400094, India*

(Received 28 July 2023; revised 3 October 2023; accepted 25 October 2023; published 27 November 2023)

The neutron emission, extensively used as a clock to measure fission delay, is not fully understood. There are ambiguities in interpretation of experimental results at higher energies and a dearth of information at low energies. In order to address these issues, a measurement of pre-scission neutron multiplicity (ν_{pre}) for $^7\text{Li} + ^{203}\text{Tl}$ at low energy ($E^* = 43.7\text{ MeV}$) have been carried out. The statistical model calculations incorporating shell corrections, constrained by fitting fission excitation functions down to energies near fission threshold, underestimate the experimental ν_{pre} values. At the energy of the present measurement, dynamical effects are found to be negligible. This would imply large emission of neutrons at the instant of neck rupture. More theoretical and experimental investigations are required to understand the behavior of low density neutron rich nuclear matter at the neck region.

DOI: [10.1103/PhysRevC.108.054609](https://doi.org/10.1103/PhysRevC.108.054609)**I. INTRODUCTION**

The fission of atomic nuclei, one of the most complex yet fascinating phenomena in nuclear physics, involves drastic rearrangement of its constituents and changes in shape governed by the structural and dynamical properties [1–3]. This journey encompasses several stages, namely, starting from equilibrium deformation to crossing over the saddle point, descent from saddle to scission, and post-scission. Behavior of the system near the scission point can be also distinctly different from the aforementioned stages, requiring separate treatment. In case of heavy-ion induced fission, the compound nucleus (CN) formation part might also be significant. Among many observables, the particles emitted during fission are of great interest as they provide insights into the potential energy landscape as well as dynamical evolution. However, the particle emission mechanisms are not fully understood. Particularly, the near scission emission is a subject of active debates [4–7], as it can be used as a probe to understand the low density neutron-rich nuclear matter.

To describe the mechanism of fission, Bohr and Wheeler [8] identified the saddle point, having the least number of states along the fission path, as the transition state. Assuming transition states are in thermal equilibrium, the statistical competition between neutron (particle) emission and fission was described. On the other hand, Kramers [9] modeled the fission process as diffusion over the barrier implying slowing down of fission process due to dissipation. As a consequence,

a decrease in fission probability and increase in particle multiplicities were expected. Neutron emission, being the most abundant, has been extensively used in the past [10,11] to study the dynamical evolution during the fission process. Neutron emission takes place from all the stages of fission discussed earlier. While pre- and post-scission contributions can be kinematically separated, estimation of near-scission contribution is difficult as its emission characteristics are similar to that of pre-scission emission. Low energy measurements, where the effects of dissipation (dynamics) is not expected to be significant and the parameters for the statistical competition between fission and neutron emission are constrained well, could be a useful tool to infer near-scission emission.

The shell corrections to the smoothly varying liquid drop (LD) surface play a vital role in fission. Incorporation of shell corrections successfully explained the observed asymmetric mass distributions, existence of fission isomers, and near constancy of the fission barrier height (B_f) in case of actinides. This also led to the exciting prediction of the superheavy island. Yet the evolution of the shell correction with deformation and temperature is not completely understood. In that scenario, the understanding of the fission process of ^{210}Po , characterized by comparable ($\approx 11\text{ MeV}$) ground state shell correction (Δ_n) and LD fission barrier (B_f^{LD}), might shed more light into it.

There are several studies involving ^{210}Po . Both statistical and dynamical model calculations neglecting the shell corrections [12–15] reproduce the available experimental fission excitation functions and the pre-fission neutron multiplicity (ν_{pre}) data at higher excitation energies. However, it was revealed that the cumulative fission probability at those excitation energies (E^*) is not sensitive to the correlated variation of the statistical model (SM) parameters [16,17]. A simultaneous SM fitting of the experimental fission excitation functions

*kmahata@barc.gov.in

†Present address: Department of Physics, SIES College of Arts, Science and Commerce, Mumbai 400 022, India.

‡Deceased.

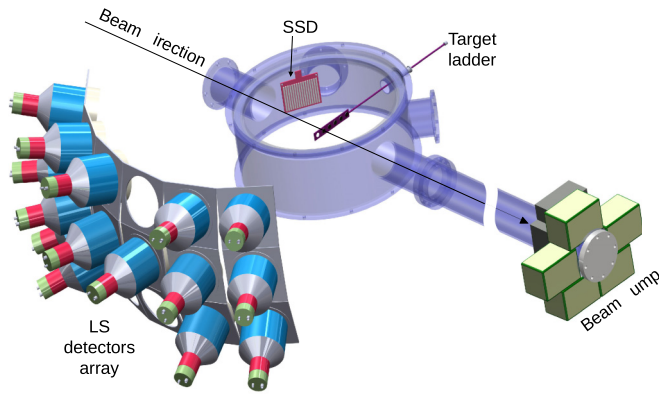


FIG. 1. The schematic of the experimental setup consists of a silicon strip detector (SSD) for detection of fission fragments and an array of 15 liquid scintillator (LS) detectors for neutron detection.

and the v_{pre} values using a consistent prescription for level densities and fission barrier resulted in very large shell corrections at the saddle point [17,18]. However, the analysis of the fission excitation functions measured down to energies near the fission barrier in light-ion (p , α) induced reactions excludes the possibility of any significant shell correction at the saddle point [19]. It was also observed that the v_{pre} values extracted from the experimental excitation functions in the light-ion induced fission of the neighboring Po isotopes are much lower than those estimated from the neutron energy spectra [12]. Thus, measurement of neutron spectra in fission of ^{210}Po at still lower energies, challenging due to low cross sections, might help in resolving these discrepancies.

In this article, we present the results of v_{pre} measurement for $^7\text{Li} + ^{203}\text{Tl}$ at $E^* = 43.7$ MeV. SM calculations considering excitation energy dependent shell corrections have been performed to interpret the present result along with the experimental data available at higher excitation energies for the same compound nucleus.

II. EXPERIMENTAL DETAILS

The experiment was carried out at the BARC - TIFR Pelletron - LINAC facility, Mumbai. Pulsed ^7Li beam of 40 MeV was bombarded on a 0.9 mg/cm^2 thick ^{203}Tl target with carbon backing. The energy loss in half-thickness of the target (104 keV) has been subtracted while calculating E^* . The schematic of the experimental setup is shown in Fig. 1. A $140\ \mu\text{m}$ thick single-sided silicon strip detector (SSD) having area of $5 \times 5\text{ cm}^2$ and 16 strips was kept at a distance of 7.6 cm from the target to detect the fission fragments. The detector was kept at an angle 150° to cover near 0° to 90° relative angles between the fragment and neutron emission directions. The total angular coverage of the detector was about 36.2° . The 16 energy signals from the front side along with the common energy signal from the back side were acquired from SSD.

The neutrons were detected using an array consisting of 15 EJ301 liquid scintillators [20]. As shown in Fig. 1, the array has provision to mount detectors at a distance of 70 cm from the center of the target in three layers separated by 16° (ϕ).

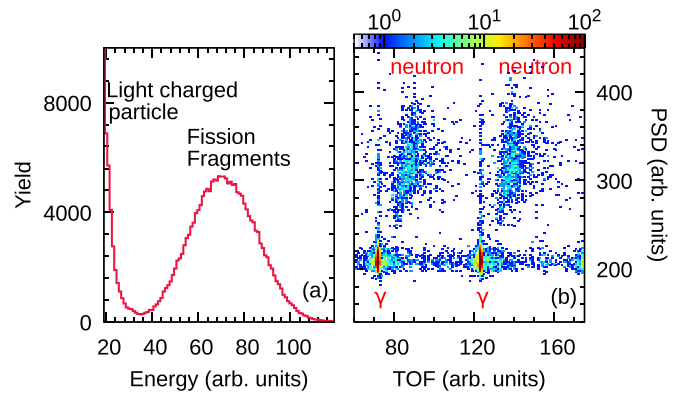


FIG. 2. (a) A typical energy spectrum recorded in one of the strips of the silicon strip detector. (b) Pulse shape discrimination (PSD) vs. time of flight (TOF) spectrum from one of the liquid scintillator detectors.

The most forward and backward scintillators were kept at 58.3° and 143.3° with respect to beam axis, respectively. Each neutron detector has a 5 in. diameter and 2 in. thickness, and is coupled to a 5 in. diameter photomultiplier tube. A threshold of 200 keV equivalent-electron (keVee), estimated using the standard γ -ray ^{137}Cs and ^{60}Co sources, was applied in the pulse height for neutron detection. The beam dump, placed at a distance of ≈ 3.4 meter from target, was adequately shielded using paraffin and lead blocks to attenuate the neutrons and γ rays emitted towards the scintillators. Time-of-flight (TOF), pulse shape discrimination (PSD), and pulse height information were acquired for neutrons. A radiofrequency (RF) signal with every alternate beam pulse was available from the accelerator to mark their arrival. The time interval between two beam pulses was 106.7 ns with a pulse width of about 0.8 ns. For better time resolution, the data acquisition was triggered by the RF signal filtered by fission trigger generated from the common signal of the strip detector.

III. DATA ANALYSIS

As shown in Fig. 2(a), the fission fragments can be clearly separated from light charged particles from the acquired energy spectrum. A total of 3.5×10^6 fission events were recorded in the experiment. Significant incomplete fusion (fragment capture) cross section have been observed for the $^7\text{Li} + ^{205}\text{Tl}$ system [21]. However, fragment capture forms less fissile composite system at lower excitation energy. Thus, it is not expected to contribute significantly to fission channel and influence the present measurement. As shown in Fig. 2(b), clean selection of neutron events was possible from the TOF vs. PSD plot.

The TOF calibrations were done using the position of the γ peaks corresponding to two beam bunches. The neutron energy (E_n) spectra, in coincidence with fission fragments, are obtained from the calibrated TOF. The neutron detection efficiency of the scintillators were estimated using a Monte Carlo simulation code, which was already validated for these scintillators [22]. Since the fission probability at the measured energy is very small, four strips were combined together to get

TABLE I. The results obtained from moving source fit.

E^* (MeV)	ν_{pre}	T_{pre} (MeV)	ν_{post}	T_{post} (MeV)
43.7	0.94 ± 0.08	1.33 ± 0.04	1.51 ± 0.03	1.01 ± 0.02

better statistics in the neutron energy spectra. Also, the neutrons spectra in scintillators mounted at same θ (but different ϕ) were combined together in order to improve the statistics. Thus, there are 24 neutron spectra corresponding to different fragment and neutron detection angles.

The measured neutron spectra have contributions from three moving sources, namely the slowly recoiling pre-scission compound nucleus and two fully accelerated post-scission fission fragments [detected fragment (DF) and complementary fragment (CF)] with high kinetic energy. Near-scission contribution, if any, will have the same characteristics as that of the compound nucleus. As the present system is populated using very asymmetric entrance channel, the compound nucleus formation time and neutron emission from this stage are expected to be negligible [11,23]. The pre- and post-scission components of neutron multiplicities (i.e., ν_{pre} and ν_{post}) and respective temperatures (T_{pre} and T_{post}) are obtained from the measured neutron energy spectra by using a moving source least-square fitting procedure. Simultaneous fits to all 24 multiplicity spectra over a wide range of relative angles between the sources and the emitted neutrons were obtained using the following expression [24]:

$$\frac{d^2v}{dE_n d\Omega} = \sum_i \frac{\nu_i \sqrt{E_n}}{2(\pi T_i)^{3/2}} e^{-\frac{E_n - 2\sqrt{E_n E_i/A_i} \cos \theta_i + E_i/A_i}{T_i}}, \quad (1)$$

where T_i and E_i/A_i represent the temperature, kinetic energy per nucleon of the neutron emitting sources, respectively. The relative angle between the velocity vectors of the source and the emitted neutron in the laboratory frame is denoted as θ_i . The multiplicities and the temperature for both the fragments were assumed to be the same. The kinetic energy of the fragments and the emission angle of the complementary fragments were estimated using the Viola systematics for symmetric fission [25].

IV. RESULTS AND DISCUSSION

Typical neutron energy spectra, essential to illustrate the variations of different contributions due to kinematic focusing, are shown in Fig. 3 along with the moving source fits. All the energy spectra can be found in the Supplemental Material [26]. The energy integrated neutron yields as a function of relative angle between the detected fragment and the neutron (θ_{nDF}) for all 24 combinations are compared with results of the moving source fit in Fig. 4. The contributions of the detected and complementary fragments are observed to peak around 0° and at folding angle, respectively, due to focusing effect. The slowly varying compound nuclear contribution (ν_{pre}) is found to dominate in the valley between the two peaks, which was covered well in present measurement. The parameters of the moving source fit are listed in Table I.

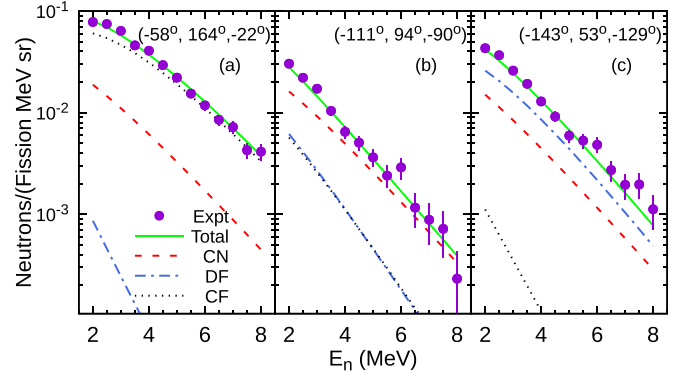


FIG. 3. Typical neutron energy spectra along with the moving source fits. The compound nucleus (CN), detected fragment (DF), and complementary fragments (CF) contributions are also shown. The numbers in brackets represent the angle of neutron emission with respect to the beam, DF, and CF in laboratory frame, respectively.

The extracted value of T_{pre} agrees well with the estimated temperature of the compound nucleus using the relation $T = \sqrt{E^*/\tilde{a}_n}$. The asymptotic value of level density parameter (\tilde{a}_n) is taken as $A_{\text{CN}}/9$ in the present study. The value of T_{post} is also consistent with the estimated available energy for excitation of the fragments. In the case of $^{12}\text{C} + ^{198}\text{Pt}$ [18], the values of ν_{post} and T_{post} were observed to be nearly constant over the measured excitation energy range. The same behavior is found to continue in the present study.

To interpret the experimental results, the statistical model calculations have been performed using the PACE code [27] with a consistent prescription to incorporate shell corrections in the level density and fission barrier [12,19] for the decay of ^{210}Po , populated in α , ^7Li , ^{12}C , and ^{18}O induced reactions. The fusion spin distributions were calculated using the CCFULL code [28] after reproducing the experimental fusion excitation functions [29–31] for ^{12}C and ^{18}O induced

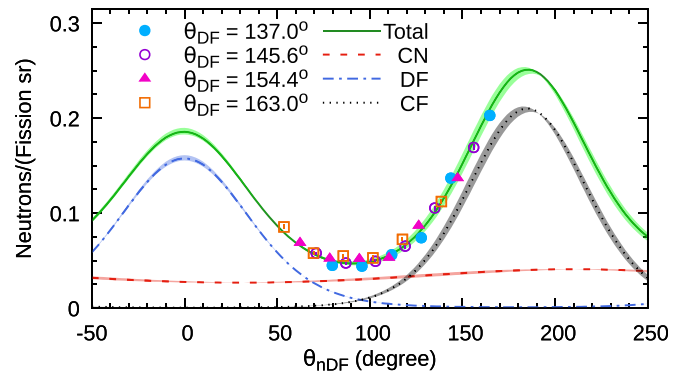


FIG. 4. The energy integrated neutron yields plotted as function of relative angle (θ_{nDF}) between the emitted neutron and detected fragment (DF) for different angular bins of DF (θ_{DF}). The results of moving source fit for compound nucleus (CN), detected fragment (DF), complementary fragment (CF), and the total correspond to mean fragment angle ($\theta_{DF} = 150^\circ$). The shaded region represents the variations in the contributions considering the range of fragment detection angles.

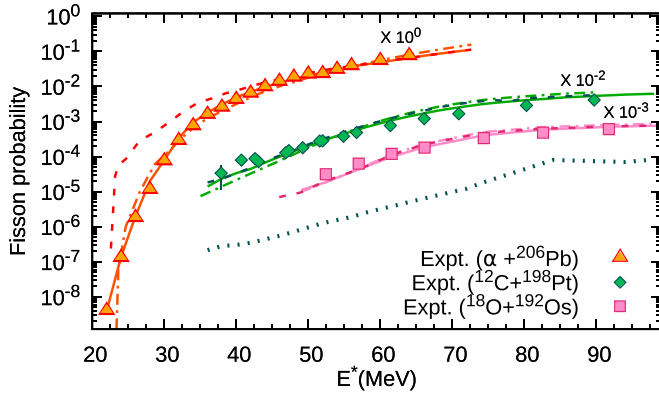


FIG. 5. The experimental fission probabilities for ^{210}Po in α [32], ^{12}C [29,30], and ^{18}O [29,31] induced reactions are compared with the results of different types of statistical model calculations (see text for details). The continuous, dot-dashed and dashed lines correspond to Types I:A, II:A, and II:B calculations, respectively. The dotted line corresponds to Type-I:B calculation for $^{12}\text{C} + ^{198}\text{Pt}$ reaction. The probabilities are scaled for representation purpose.

reactions. As the beam energies are much above the Coulomb barrier, the fusion cross sections are taken from the Bass model [33] for α and ^7Li -induced reactions. The angular momentum dependent LD part of the fission barrier [$B_f^{LD}(J)$] and rotational energy [$E_{\text{rot}}(J)$] are taken from the rotating finite range model (RFRM) [34]. The intrinsic excitation energy is given as $E_x = E^* - E_{\text{rot}}(J) - \delta_p$, where δ_p is pairing correction. The values of Δ_n are taken from Ref. [35]. Both realistic gradual (Type-I) and complete (Type-II: LD) washings out of shell corrections have been considered in the present analysis. The square of entropy for the equilibrium deformation are calculated as $S_n^2 = 4\tilde{a}_n[E_x + \Delta_n(1 - e^{-\eta E_x})]$ and $S_n^2 = 4\tilde{a}_n[E_x + \Delta_n]$ for Type-I and Type-II, respectively. The square of entropy for the saddle point is given as $S_f^2 = 4\tilde{a}_f[E_x + \Delta_n - B_f^{LD}]$ for both options. More details about the level density ($\rho_{n,f}(E_x) \sim \exp[S_{n,f}(E_x)]$) prescription can be found in Refs. [12,19]. A scaling factor to the RFRM $B_f^{LD}(J)$ and the ratio of the level density parameter at saddle point to that at equilibrium deformation (\tilde{a}_f/\tilde{a}_n) were varied to reproduce the experimental results.

The results of the SM calculations are compared with the available experimental fission excitation functions and ν_{pre} data in Figs. 5 and 6, respectively. Fits to the excitation functions and ν_{pre} data are labeled as ‘A’ and ‘B’, respectively. All the fission excitation functions could be simultaneously reproduced well in Type-I:A [$\tilde{a}_f/\tilde{a}_n = 1.035$ and $B_f^{LD}(0) = 11.3$ MeV]. The corresponding total fission barrier, $B_f^{LD}(0) - \Delta_n = 21.9$ MeV matches well with the predictions of the macroscopic-microscopic finite-range liquid-drop model [36]. While it underpredicts the pre-scission ν_{pre} data even at the lowest energy, the results are found to be in good agreement with ν_{pre} values (filled triangles) extracted in Ref. [12] from the experimental fission excitation functions of Po isotopes in $^3,^4\text{He}$ induced reactions [37]. As the fission probability is less influenced by the post-saddle phenomena, the ν_{pre} values extracted from the experimental fission excitation functions

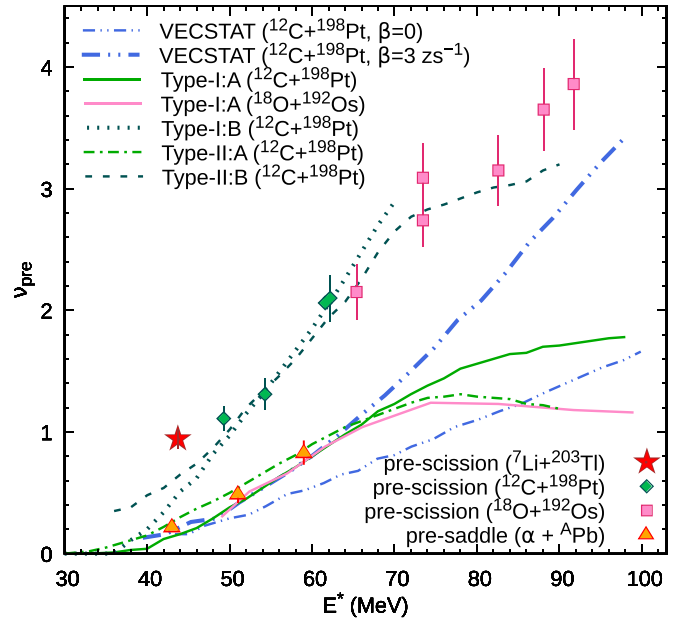


FIG. 6. The comparison of experimentally measured ν_{pre} values for ^{210}Po in ^7Li (present data), ^{12}C [18,38], and ^{18}O [39] induced reactions. The statistical model predictions in Types I:A, I:B, II:A, and II:B calculations for ^{12}C and Type-I:A calculation for ^{18}O induced reactions are shown (see text for details). The predictions of the VECSTAT code with $\beta = 0, 3 \text{ zs}^{-1}$ from Ref. [40] are also plotted for comparison. The pre-saddle ν_{pre} extracted in Ref. [12] are also shown.

can be considered as pre-saddle fission multiplicities. In the SM, the fission probability is mainly governed by the level density at the saddle point. Thus, the ν_{pre} values predicted by the SM also corresponds to pre-saddle part only. Hence, the good agreement between the SM prediction and the ν_{pre} values estimated from the excitation functions reaffirms the reliability of the SM calculation. An unreasonably small value of \tilde{a}_f/\tilde{a}_n (0.78) is required to reproduce the experimental pre-scission multiplicities (Type-I:B). Owing to much steeper fall, it even fails to reproduce the lowest energy data from the present measurement. Further, it underpredicts the experimental fission probabilities by several orders of magnitude. The predicted ν_{pre} values in Type-II:A [$\tilde{a}_f/\tilde{a}_n = 1.085$ and $B_f^{LD}(0) = 12.3$ MeV], which also fits the excitation functions, are much lower than the experimental values and agree well with Type-I:A results. It is possible to fit the ν_{pre} values as well as all the excitation functions above 45 MeV in Type-II:B [$\tilde{a}_f/\tilde{a}_n = 1.012$ and $B_f^{LD}(0) = 10.8$ MeV]. However, it fails to reproduce the ν_{pre} value from the present measurement as well as the low energy part of the α induced excitation function.

The PACE results start to exhibit the saturation behavior for $E^* > 65$ MeV, which was also observed earlier [41]. Because of the larger angular momentum brought in, the SM predicts larger fission probability and smaller values of ν_{pre} for $^{18}\text{O} + ^{192}\text{Os}$ system as compared to the $^{12}\text{C} + ^{198}\text{Pt}$ system at energies above 65 MeV. It is observed that for $E^* < 65$ MeV, the predicted ν_{pre} values for all the entrance channels

considered are similar. The results for α and ${}^7\text{Li}$ induced reactions are not shown for clarity.

The results of the SM code VECSTAT from Ref. [40] are also shown in Fig. 6. In VECSTAT the effects of collective enhancement in level density, orientation (K) degree of freedom, and dissipation are also considered. It is worth noting that neutron emission during saddle-to-scission motion was also taken into account in this calculation. The VECSTAT results for 3zs^{-1} as a reduced dissipation coefficient (β) are found to agree well with the PACE results below $E^* \approx 65$ MeV. It is important to note that at the excitation energy of the present measurement, the VECSTAT predicts similar values of ν_{pre} with and without dissipation, indicating the absence of any significant effect of dissipation at these low energies. The fission excitation function and ν_{pre} values with $E^* > 50$ MeV for ${}^{210}\text{Po}$ have been reproduced by dynamical model calculations using macroscopic potential energy, neglecting microscopic shell corrections [13,14]. Even the same can be reproduced by the present SM calculation assuming complete washing out of shell corrections (Type-II:B). However, such a calculation is not consistent with the low energy light-ion induced fission excitation functions for the same compound nucleus as shown in Fig. 5.

From the above, it can be concluded that the excess ν_{pre} observed is not due to pre-saddle or post-saddle dynamics. Pre-actinide nuclei are well deformed at the saddle [42] and the saddle-to-scission motion is expected to be quick without contributing significantly to the observed ν_{pre} . In fact, it was also shown [43] that the transient delay and the saddle-to-scission time are negligibly small as compared to statistical fission lifetime when the fission barrier is much larger than the temperature as the present case. The fissility of ${}^{210}\text{Po}$ (0.71) and the charge product in entrance channels considered (≤ 608) are low. The fission excitation functions for same compound nucleus populated using p , α , ${}^{12}\text{C}$, and ${}^{18}\text{O}$ as projectile could be explained using the same SM framework [19]. The ν_{pre} values belonging to different entrance channels are found to increase monotonously with excitation energy. Thus, the entrance channel dynamics or the CN formation stage is also not expected to have significant influence on the present result, particularly the present system as large asymmetry involved in the entrance channel.

Understanding the near-scission emission also known as ternary fission is a longstanding problem [5,6,44,45]. Emission of the charged particle from the neck region has a characteristic angular and energy distributions due to Coulomb repulsion of the fragments and have been studied extensively. No such advantage is available for the neutron as it has no charge. Thus experimentally it is challenging to

extract near-scission neutron contribution reliably and for it to remain obscure. Though there are large uncertainties, the presence of 10–30% near-scission neutrons per fission have been reported [45]. A recent phenomenological dynamical scission point model calculation also suggests significant scission contribution to neutron multiplicity [7]. About 0.78 near scission neutrons per fission will provide good agreement with the calculations using $\beta = 3\text{zs}^{-1}$ over the entire energy range in the present case. Such a possibility will impact the study of dissipative dynamics at higher excitation energies and the behavior of low density neutron rich nuclear matter at the neck connecting the fragments [4,5,46].

V. SUMMARY

Pre-fission neutron multiplicities for the ${}^7\text{Li} + {}^{203}\text{Tl}$ reaction, populating ${}^{210}\text{Po}$ at $E^* = 43.7$ MeV, have been determined from the measured neutron spectra. While the statistical model calculations with realistic gradual (Type-I:A) and complete (Type-II:A) washings out of shell corrections reproduce the fission excitation functions down to excitation energy near the fission threshold and the pre-saddle ν_{pre} , those underpredict the pre-scission ν_{pre} measured in the present study and the data for the same compound nucleus available at higher excitation energies substantially. Attempts to reproduce the pre-scission ν_{pre} (Type-I:B and II:B), fails to reproduce the data from the present measurement and all the excitation functions simultaneously. At the excitation energy of the present measurement, the effect of dissipation in the pre-saddle as well as saddle-to-scission stages are found to be negligibly small. The CN formation stage is also not expected to contribute significantly as large asymmetry involved in the entrance channels, particularly the present system. Thus the excess ν_{pre} can be attributed to the near-scission emission. The present study suggests that the measurements at low energies, where the statistical model parameters can be constrained well and the effect of dissipation can be neglected, could be used as a tool to study near-scission emission and will give new impetus for more theoretical and experimental investigations, which has implications on studies of dissipative nuclear dynamics and low density neutron rich matter.

ACKNOWLEDGMENTS

We acknowledge the assistance received from Mr. P. Patale during the experiment. We thank accelerator staff for smooth operation. One of the authors (S.D.) acknowledges financial support from Department of Science and Technology, India through the INSPIRE fellowship.

-
- [1] R. Vandenbosch and J. Huizenga, *Nuclear Fission* (Academic, New York, 1973).
 - [2] N. Schunck and D. Regnier, *Prog. Part. Nucl. Phys.* **125**, 103963 (2022).
 - [3] K.-H. Schmidt and B. Jurado, *Rep. Prog. Phys.* **81**, 106301 (2018).
 - [4] J. B. Natowitz, H. Pais, and G. Röpke, *Phys. Rev. C* **107**, 014618 (2023).
 - [5] Z. X. Ren, D. Vretenar, T. Nikšić, P. W. Zhao, J. Zhao, and J. Meng, *Phys. Rev. Lett.* **128**, 172501 (2022).
 - [6] J. P. Lestone, *Phys. Rev. C* **70**, 021601(R) (2004).
 - [7] N. Carjan, I. Stetcu, M. Rizea, and A. Bulgac, *EPJ Web Conf.* **256**, 00004 (2021).
 - [8] N. Bohr and J. A. Wheeler, *Phys. Rev.* **56**, 426 (1939).
 - [9] H. A. Kramers, *Physica* **7**, 284 (1940).
 - [10] D. Hilscher and H. Rossner, *Ann. Phys. Fr.* **17**, 471 (1992).

- [11] A. Saxena, A. Chatterjee, R. K. Choudhury, S. S. Kapoor, and D. M. Nadkarni, *Phys. Rev. C* **49**, 932 (1994).
- [12] K. Mahata and S. Kailas, *Phys. Rev. C* **95**, 054616 (2017).
- [13] C. Schmitt, K. Mazurek, and P. N. Nadtochy, *Phys. Lett. B* **737**, 289 (2014).
- [14] D. Arora, P. Sugathan, and A. Chatterjee, *Chin. Phys. C* **47**, 034003 (2023).
- [15] S. G. McCalla and J. P. Lestone, *Phys. Rev. Lett.* **101**, 032702 (2008).
- [16] K. Mahata, S. Kailas, A. Shrivastava, A. Chatterjee, A. Navin, P. Singh, S. Santra, and B. S. Tomar, *Nucl. Phys. A* **720**, 209 (2003).
- [17] K. Mahata, S. Kailas, and S. S. Kapoor, *Phys. Rev. C* **74**, 041301(R) (2006).
- [18] K. S. Golda, A. Saxena, V. K. Mittal, K. Mahata, P. Sugathan, A. Jhingan, V. Singh, R. Sandal, S. Goyal, J. Gehlot, A. Dhal, B. R. Behera, R. K. Bhowmik, and S. Kailas, *Nucl. Phys. A* **913**, 157 (2013).
- [19] K. Mahata, S. Kailas, and S. S. Kapoor, *Phys. Rev. C* **92**, 034602 (2015).
- [20] P. C. Rout, A. Gandhi, T. Basak, R. G. Thomas, C. Ghosh, A. Mitra, G. Mishra, S. P. Behera, R. Kujur, E. T. Mirgule, B. K. Nayak, A. Saxena, S. Kumar, and V. M. Datar, *J. Sci. Instrum.* **13**, P01027 (2018).
- [21] V. V. Parkar, M. Prasanna, R. Rathod, V. Jha, S. K. Pandit, A. Shrivastava, K. Mahata, K. Ramachandran, R. Palit, M. S. R. Laskar, B. J. Roy, B. Kanagalekar, and B. G. Hegde, *Phys. Rev. C* (to be published).
- [22] V. V. Desai, B. K. Nayak, A. Saxena, S. V. Suryanarayana, and R. Capote, *Phys. Rev. C* **92**, 014609 (2015).
- [23] C. Schmitt, K. Mazurek, and P. N. Nadtochy, *Phys. Rev. C* **97**, 014616 (2018).
- [24] D. Hilscher, J. R. Birkelund, A. D. Hoover, W. U. Schröder, W. W. Wilcke, J. R. Huizenga, A. C. Mignerey, K. L. Wolf, H. F. Breuer, and V. E. Viola, Jr., *Phys. Rev. C* **20**, 576 (1979).
- [25] V. E. Viola, K. Kwiatkowski, and M. Walker, *Phys. Rev. C* **31**, 1550 (1985).
- [26] See Supplemental Material at <http://link.aps.org/supplemental/10.1103/PhysRevC.108.054609> for all neutron multiplicity spectra along with results of moving source fit.
- [27] A. Gavron, *Phys. Rev. C* **21**, 230 (1980).
- [28] K. Hagino, N. Rowley, and A. T. Kruppa, *Comput. Phys. Commun.* **123**, 143 (1999).
- [29] J. van der Plicht, H. C. Britt, M. M. Fowler, Z. Fraenkel, A. Gavron, J. B. Wilhelmy, F. Plasil, T. C. Awes, and G. R. Young, *Phys. Rev. C* **28**, 2022 (1983).
- [30] A. Shrivastava, S. Kailas, A. Chatterjee, A. Navin, A. M. Samant, P. Singh, S. Santra, K. Mahata, B. S. Tomar, and G. Pollarolo, *Phys. Rev. C* **63**, 054602 (2001).
- [31] R. J. Charity, J. R. Leigh, J. J. M. Bokhorst, A. Chatterjee, G. S. Foote, D. J. Hinde, J. O. Newton, S. Ogaza, and D. Ward, *Nucl. Phys. A* **457**, 441 (1986).
- [32] L. G. Moretto, K. X. Jing, R. Gatti, G. J. Wozniak, and R. P. Schmitt, *Phys. Rev. Lett.* **75**, 4186 (1995).
- [33] R. Bass, *Phys. Rev. Lett.* **39**, 265 (1977).
- [34] A. J. Sierk, *Phys. Rev. C* **33**, 2039 (1986).
- [35] P. Möller, A. J. Sierk, T. Ichikawa, A. Iwamoto, R. Bengtsson, H. Uhrenholt, and S. Åberg, *Phys. Rev. C* **79**, 064304 (2009).
- [36] P. Möller, A. J. Sierk, T. Ichikawa, A. Iwamoto, and M. Mumpower, *Phys. Rev. C* **91**, 024310 (2015).
- [37] K. Jing, I. Fission probabilities, fission barriers, and shell effects. II. Particle structure functions, Ph.D. thesis, University of California at Berkeley, 1999.
- [38] C. Sharma, B. R. Behera, Shruti, Amit, B. Rohila, A. Kaur, Subodh, N. Dhanda, A. Kumar, P. Sugathan, A. Jhingan, K. S. Golda, N. Saneesh, M. Kumar, H. Arora, D. Arora, and H. P. Sharma, *Phys. Rev. C* **107**, 064615 (2023).
- [39] J. O. Newton, D. J. Hinde, R. J. Charity, J. R. Leigh, J. J. M. Bokhorst, A. Chatterjee, G. S. Foote, and S. Ogaza, *Nucl. Phys. A* **483**, 126 (1988).
- [40] T. Banerjee, S. Nath, and S. Pal, *Phys. Rev. C* **99**, 024610 (2019).
- [41] D. J. Hinde, R. J. Charity, G. S. Foote, J. R. Leigh, J. O. Newton, S. Ogaza, and A. Chatterjee, *Nucl. Phys. A* **452**, 550 (1986).
- [42] S. Cohen and W. J. Swiatecki, *Ann. Phys.* **22**, 406 (1963).
- [43] J. P. Lestone and S. G. McCalla, *Phys. Rev. C* **79**, 044611 (2009).
- [44] N. Feather, *Proceedings of the Second IAEA Symposium on Physics and Chemistry of Fission* (IAEA, Vienna, 1969), pp. 83–105.
- [45] I. Halpern, *Annu. Rev. Nucl. Sci.* **21**, 245 (1971).
- [46] S. Wuenschel, H. Zheng, K. Hagel, B. Meyer, M. Barbui, E. J. Kim, G. Röpke, and J. B. Natowitz, *Phys. Rev. C* **90**, 011601(R) (2014).